ELSEVIER

Catalysis Today 77 (2003) 385–406

CATALYSIS TODAY

www.elsevier.com/locate/cattod

Some contributions of electron microscopy to the characterisation of the strong metal–support interaction effect

S. Bernal*, J.J. Calvino, M.A. Cauqui, J.M. Gatica, C. López Cartes, J.A. Pérez Omil, J.M. Pintado

Departamento de Ciencia de los Materiales e Ingeniería Metalúrgica y Química Inorgánica, Facultad de Ciencias, Universidad de Cádiz, Campus Rio San Pedro, Apartado 40, Puerto Real, 11510 Cádiz, Spain

Abstract

The contribution of electron microscopy techniques to establishing the existence and actual nature of the metal–support interaction effects occurring in a variety of supported metal catalysts is reviewed. Data pertaining to systems based on both classic reducible supports like TiO_2, CeO_2 or some ceria-based mixed oxides, and several others generally considered as non-reducible oxides, like La_2O_3 or SiO_2, are presented and discussed. The specific temperature and chemical conditions under which strong metal–support interaction phenomena are onset or reverted in each case are also analysed.

The whole set of data presented and discussed here clearly shows that the electron microscopy techniques have made an outstanding contribution to the characterisation of the strong metal/support interaction effects exhibited by different metal/oxide systems. Likewise, it is demonstrated that this powerful family of techniques has very much helped to discriminating between *true* SMSI-like phenomena, as originally defined by Tauster et al., and several other *apparent* effects which, though at a first sight show some of the chemical, nano-structural and/or catalytic characteristics of the SMSI effect, have a neatly different origin.

Keywords: Electron microscopy; Characterisation; Strong metal–support interaction

1. Introduction

Nowadays, the electron microscopes constitute a family of very powerful catalyst characterisation techniques. All of them have a general common origin, the physical phenomena occurring when a conveniently accelerated electron beam interacts with the matter. By attaching to the microscope the appropriate detection devices, the phenomena mentioned above may be analysed, thus allowing a rich variety of information to be obtained. Essentially, the electron microscopes may provide very useful data about the textural, structural and chemical constitution of the catalysts. The main advantage of these techniques comes from the possibility of focusing the electron beam on very small areas of the samples. The development of field emission sources and their implementation in electron microscopes have allowed the generation of electron probes (nanoprobes) with diameters of the order of only a few angstroms. In this way, characterisation studies may be performed at a nano-size scale. This feature is particularly relevant in heterogeneous catalysis because of the polycrystalline and very often polyphasic nature of the catalytic materials.

In parallel with the developments which occurred both in the design of the microscopes, and in the electronic devices for their control, and data acquisition

* Corresponding author. Fax: +34-56834924.
E-mail address: serafin.bernal@ucs.es (S. Bernal).

0920-5861/02/$ – see front matter
PII: S0920-5861(02)00382-6

and processing, powerful computer simulation techniques became also available. As illustrated by the data included in this paper, the combination of both experimental and computer simulation techniques plays an essential role in the detailed interpretation of the experimental electron micrographs.

The paper focuses on some recent results about a specific phenomenon occurring in catalytic materials: the so-called strong metal–support interaction (SMSI) effect. The analysis of this particular problem illustrates some major contributions of electron microscopy to the catalyst characterisation. Though most of the results to be discussed will deal with high resolution electron microscopy (HREM), examples of how analytical studies using electron energy loss spectroscopy, or scanning electron microscopy (SEM) provide key pieces of information to understand this phenomenon are also presented.

Most of the data included in this paper correspond to experimental and calculated high resolution images. Fringe analysis of these images has been performed using fast Fourier transforms (FFTs). The results of FFT analysis are presented in the form of digital diffraction patterns (DDPs). These DDPs correspond to the log-scaled power spectra of FFT calculated from selected, squared, regions of the images. From these DDPs some crystallographic information about the imaged material can be derived. Specifically, the spacings of fringes present in the images and angles between them can be estimated within about 5% accuracy.

2. The SMSI effect in M/TiO_2 catalysts

For the past 20 years, a large number of publications have dealt with different aspects of the SMSI effect [1]. This research effort may easily be justified in terms of a fundamental understanding of such a special phenomenon, but also because of its implications in the design of specific preparation, characterisation, or catalytic applications of the metal/support systems exhibiting this effect.

Since the very first studies [1–3], the characteristics of the SMSI effect could be established in a rather precise way. Typically associated with reducible supports, it is characterised by the following major features: (1) the catalyst reduced at low temperature shows a conventional chemical behaviour. (2) Upon increasing T_{redn}, the chemisorption capability of the dispersed metal phase against the classic probe molecules like H_2 or CO is heavily disturbed (SMSI state). Likewise, substantial modifications of its catalytic behaviour are observed. (3) The phenomenon is reversible, i.e. the re-oxidation at an appropriate temperature followed by a mild re-reduction treatment allows recovering the catalyst from the SMSI state.

In the decade of 1980, the majority of the studies dealing with this effect were focused on M/TiO_2 systems [3]. The experimental conditions allowing both the induction of the SMSI state and the recovery from it were soon established. Regarding the onset of the effect, reduction, usually with flowing hydrogen, at 773 K, may be considered as a typical treatment. As far as the regeneration of the catalyst is concerned, re-oxidation in a flow of O_2 at 773 K, followed by reduction at $T \leq 573$ K, is generally accepted to induce the reversion of the phenomenon. Though specifically established for M/TiO_2 catalysts, these reference conditions have very much influenced all the ulterior studies on the effect, being almost universally applied with independence of the M/oxide system under investigation. In most cases, however, specific experiments aimed at justifying such a generalisation were lacking [4–6].

During this initial period, the likely origin of the SMSI effect was widely discussed. Two major factors were considered [3]. For some authors, the perturbations associated with the electronic interactions occurring between the dispersed metal phase and the reduced oxide support would be the determining factor. For some others, the effect had a geometric origin, i.e. upon high temperature reduction, the metal particles would become partly covered by a thin layer of the reduced support, thus blocking the chemisorption active centres at the metal surface. Regarding the latter interpretation, a number of experimental techniques, and particularly HREM [7–9], have clearly shown the occurrence of metal covering (decoration).

Figs. 1 and 2, taken from [9], show some of the experimental HREM images which have provided support to this interpretation. These images were obtained on a 2.5% Rh/TiO_2 catalyst. As Fig. 1 depicts, after reduction at 473 K a large number of nanosized metallic rhodium particles are observed distributed over the surface of both anatase and rutile support crystallites.

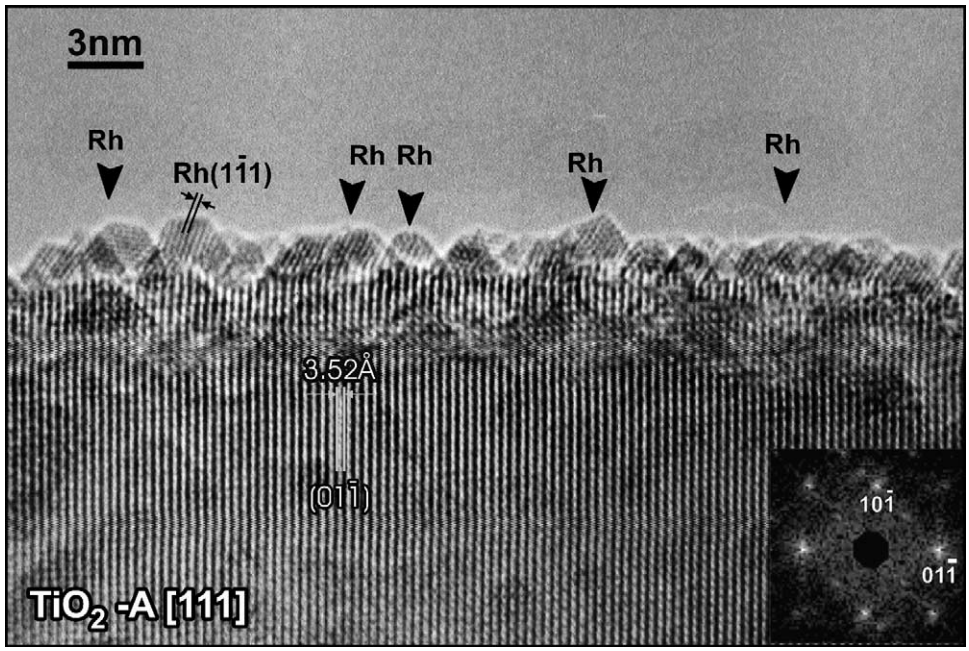

Fig. 1. HREM image of a Rh/TiO_2 catalyst reduced at 473 K, showing rhodium particles supported on an anatase crystallite.

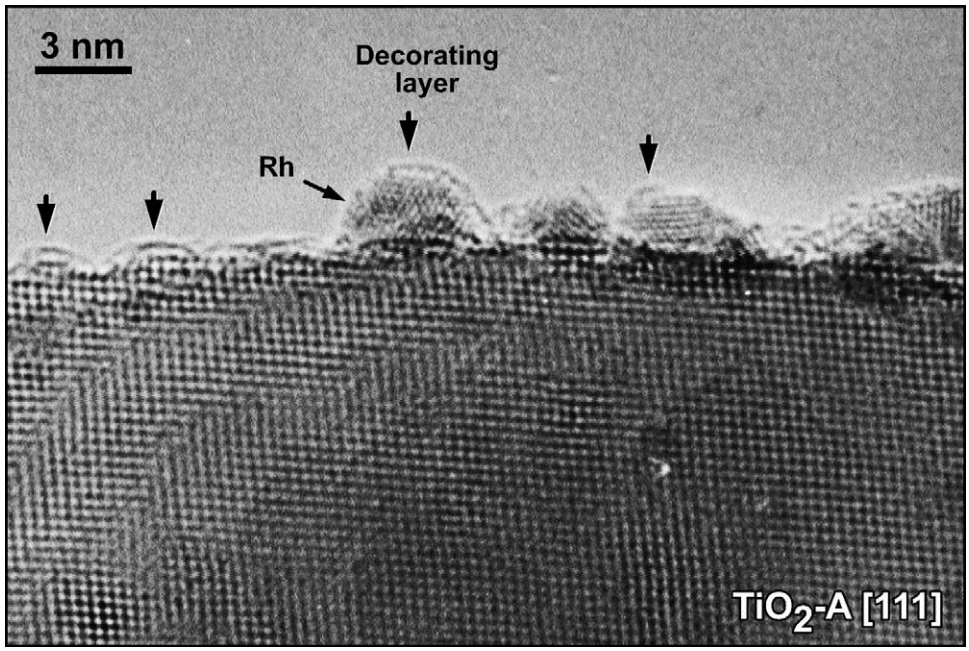

Fig. 2. HREM image of a Rh/TiO_2 catalyst reduced at 773 K. The growth of a thin amorphous layer on the metal particles (decoration) and the support is detected.

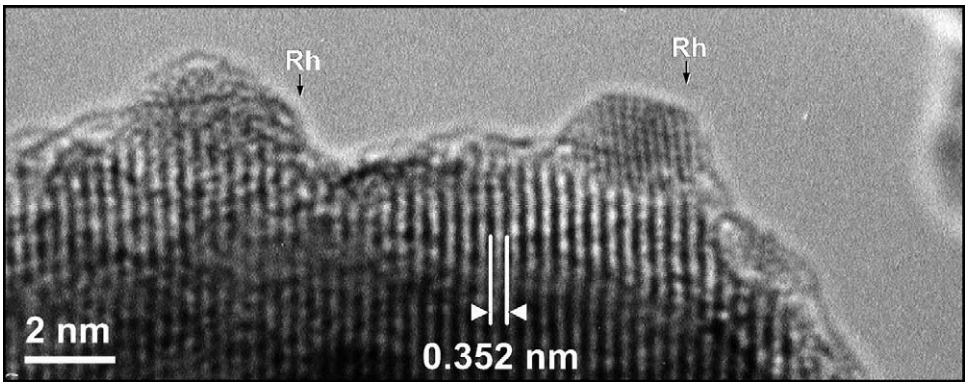

Fig. 3. Experimental image of a Rh/TiO_2 catalyst reduced at 873 K showing the co-existence of clean and partially covered metal particles.

Most of the particles are well-shaped, with morphologies close to that of truncated cubeoctahedrons. The exposed surfaces of these particles appear neatly clean.

The increase of the reduction temperature up to 773 K promotes the migration of the support over the surface of the metal particles, which in this case show, Fig. 2, a very thin covering layer. According to [9], this decoration effect does not affect the whole metal surface, even after increasing the reduction temperature up to 873 K. Fig. 3 shows an example of the partial decoration effect in this catalyst. Note in this case the presence in the image of a rhodium particle covered by the support, on the left, as well as other, on the right, with facets completely free from coverage.

In accordance with the ^{1}H-NMR spectroscopy studies carried out on a Rh/TiO_2 [10], however, the metal

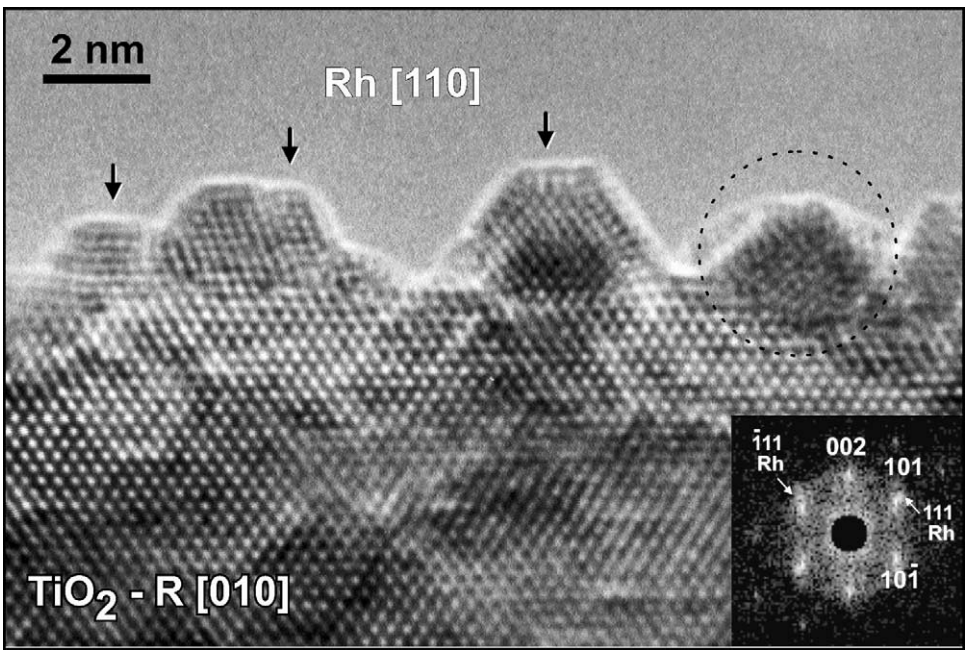

Fig. 4. HREM image of a Rh/TiO_2 catalyst reduced at 773 K and further re-oxidised at 673 K. It shows the clean rhodium particles resulting from the reversion of the decorated state.

deactivation starts to be observed at reduction temperatures well below those at which the decoration phenomena occur, thus suggesting that both electronic and geometric factors have a relevant contribution. Nowadays, the latter interpretation seems to be the most likely one. The complete inhibition of the hydrogen adsorption capability after reduction at 773 K on the 2.5% Rh/TiO_2 catalyst [9], in which only a partial decoration of the surface occurs, is also in good agreement with the ^{1}H-NMR data.

Regarding titania supported catalysts, HREM images have also provided conclusive clues about the reversibility of the decoration effect after re-oxidation at 673 K. Fig. 4 shows a representative HREM image of 2.5% Rh/TiO_2 catalyst after reduction at 773 K and further re-oxidation at 673 K. After this treatment the decoration layers are no longer present on the particles which, once again, expose clean surfaces.

3. Other M/oxide systems on which SMSI-like effects have been reported to occur

Though to a much lesser extent than titania, several other reducible oxides have also been investigated in relation to the SMSI effect. Such is the case of vanadia- or niobia-based catalysts [2,3]. Moreover, the SMSI effect has been reported to occur on Pt/SiO_2 [11] and Pd/La_2O_3 [12]. These two cases are particularly striking because the supports, SiO_2 and La_2O_3, are generally considered to be hardly reducible oxides. On Pt/SiO_2 [11], the metal deactivation effects start to be observed on the catalyst reduced for 10 h at 823 K, they becoming much stronger after a prolonged reduction treatment at 973 K. Severe reduction conditions are thus required to induce the effect. In [11], the observed deactivation is interpreted as due to the formation of a Pt–Si alloy phase, the proposal being consistent with some recent results [13,14].

Likewise, in [12] the authors interpret as due to an SMSI-like effect the peculiar chemical behaviour of a Pd/La_2O_3 catalyst reduced at a very moderate temperature: 573 K. As previously mentioned, such an interpretation is not in good agreement with the well-established redox character of lanthana. The detailed investigation performed in [15] of the evolution of the nanostructure of a 10% Rh/La_2O_3 catalyst during the different preparation steps (impregnation, drying and reduction), using both HREM and SEM microscopes, have allowed to propose an alternative interpretation to the deactivation of the chemisorption observed in catalysts supported on lanthana. This example illustrates the difference between a *true* SMSI effect, as defined by Tauster et al. [1] and some other phenomena which, in spite of showing notable

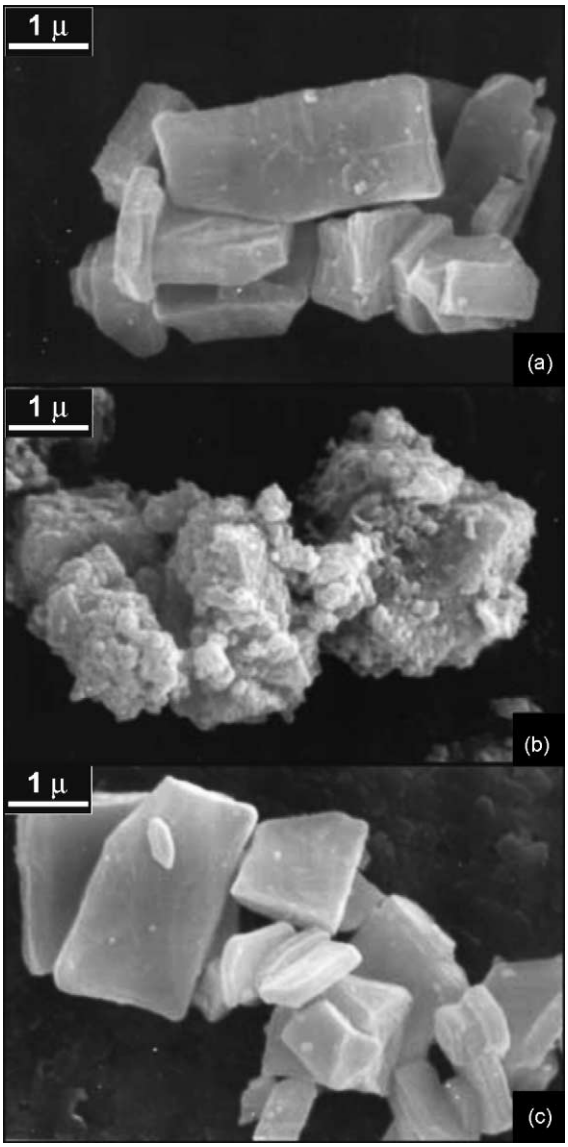

Fig. 5. SEM images corresponding to: (a) the starting Y_2O_3 support; (b) the same yttria sample further impregnated with an aqueous solution of $Rh(NO_3)_3$; and (c) the same yttria sample further impregnated with an acetone solution of $Rh(NO_3)_3$.

chemical and nano-structural similarities with it, actually have a very different origin.

According to [15], during the impregnation step a strong dissolution of the support takes places. The reaction between the highly acidic aqueous solution containing the metal precursor and the basic support is responsible of the dissolution process. SEM images like those gathered in Fig. 5 evidence the dramatic textural changes associated with the dissolution of 4f-sesquioxide supports. These textural changes are accompanied by profound chemical modifications of the support, which converts into a complex mixture of hydrated and carbonated phases.

After drying, simultaneous reprecipitation of both Rh and La ions present in solution would lead most of the metal atoms to get embedded in the bulk of the support at a very high level of dispersion. The lack of features evidencing or suggesting the presence of metal nanoparticles in HREM images recorded on catalysts reduced at low temperature, Fig. 6, supports this interpretation. Likewise the formation of a $LaRhO_3$ perovskite after heating the impregnated sample under helium at 1200 K suggests an intimate contact between Rh and La after the impregnation step, Fig. 7.

Increasing the reduction temperature in the 773–973 K range gives rise to segregation of the metal atoms out of the mixed phase and their agglomeration into larger clusters. In parallel, a deep rearrangement of the support takes place due to the thermal decomposition of the lanthanum hydroxide and hydroxycarbonate phases to La_2O_3. These changes lead finally to a catalyst in which nanosized Rh particles covered by patches of lanthana can be easily observed, Fig. 8. Both the size and number of these particles increases with reduction temperature.

HREM images recorded both on the low temperature reduced and on the high temperature calcined samples suggest a close contact of the metal phase and the support. Increasing the reduction temperature favours the decomposition of the support and, in parallel, the growth of the metallic particles. Hence, the support present on the particles on the high temperature reduced samples could be simply material dragged by the metal during the sintering process.

In other words, the support rearrangement associated with its decomposition seems to be the driving force for the decoration process. It is not necessary to relate the presence of decoration layers on the particles

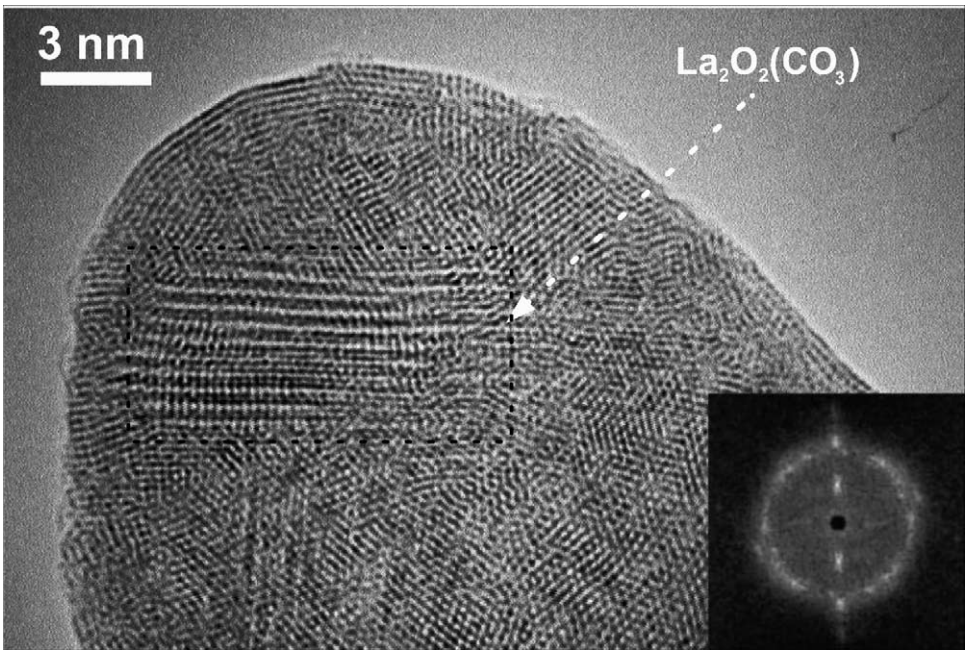

Fig. 6. HREM image depicting the structure of a 10% Rh/La_2O_3 catalyst reduced at 473 K. Inset: DDP calculated from the marked region.

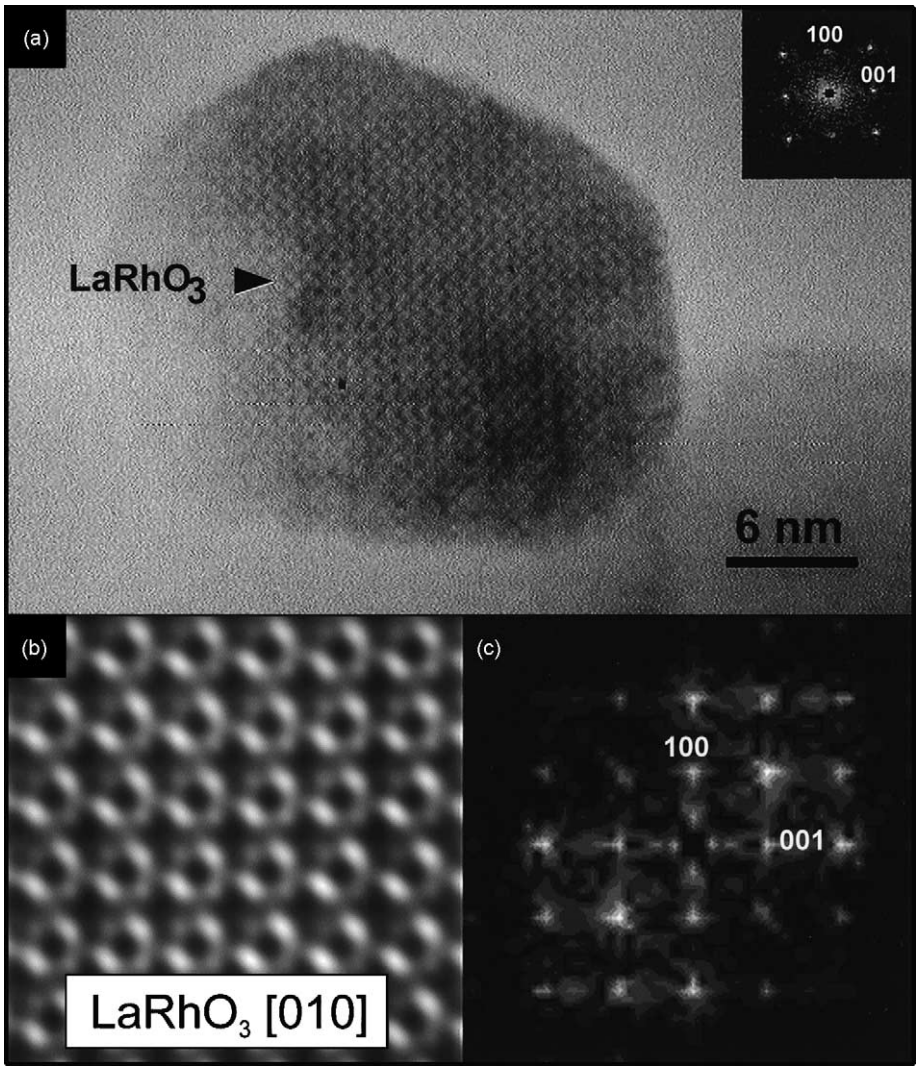

Fig. 7. (a) HREM image of a lanthana sample resulting from several impregnation cycles with aqueous solution of $Rh(NO_3)_3$ (metal loading: 10 wt.%), and further heated at 1200 K in a flow of He; (b) the inset DDP can be indexed as due to the [0 1 0] zone axis of a $LaRhO_3$ phase; simulated HREM image obtained for a 10 nm thick $LaRhO_3$ crystal 7° off the [0 1 0] zone axis; (c) DDP obtained from the calculation.

to the reduction of the support, which is in fact a very unlikely process to occur on the basis of the well-known redox chemistry of La, specially when reduction temperatures as low as 573 K are considered.

Analogous results have been obtained on other lanthanide sesquioxide supported rhodium catalysts [16]. Fig. 9 shows HREM images recorded on a 5.4% Rh/Sm_2O_3 catalyst. In this case even after reduction at 773 K, Fig. 9(a), no metal particle is still observed. Only after very high temperature treatments which allow the decomposition of the hydroxycarbonated support and sintering of the highly dispersed metal phase can small metal crystallites be observed, encapsulated by support overlayers, Fig. 9(b).

Synthesis procedures of these catalysts which overcome the dissolution of the support lead to materials in which the metal phase is present from the early stages as metal nanoparticles on the surface of the oxide, instead of getting buried into the bulk. This has been achieved by different methods [15]: (1) using

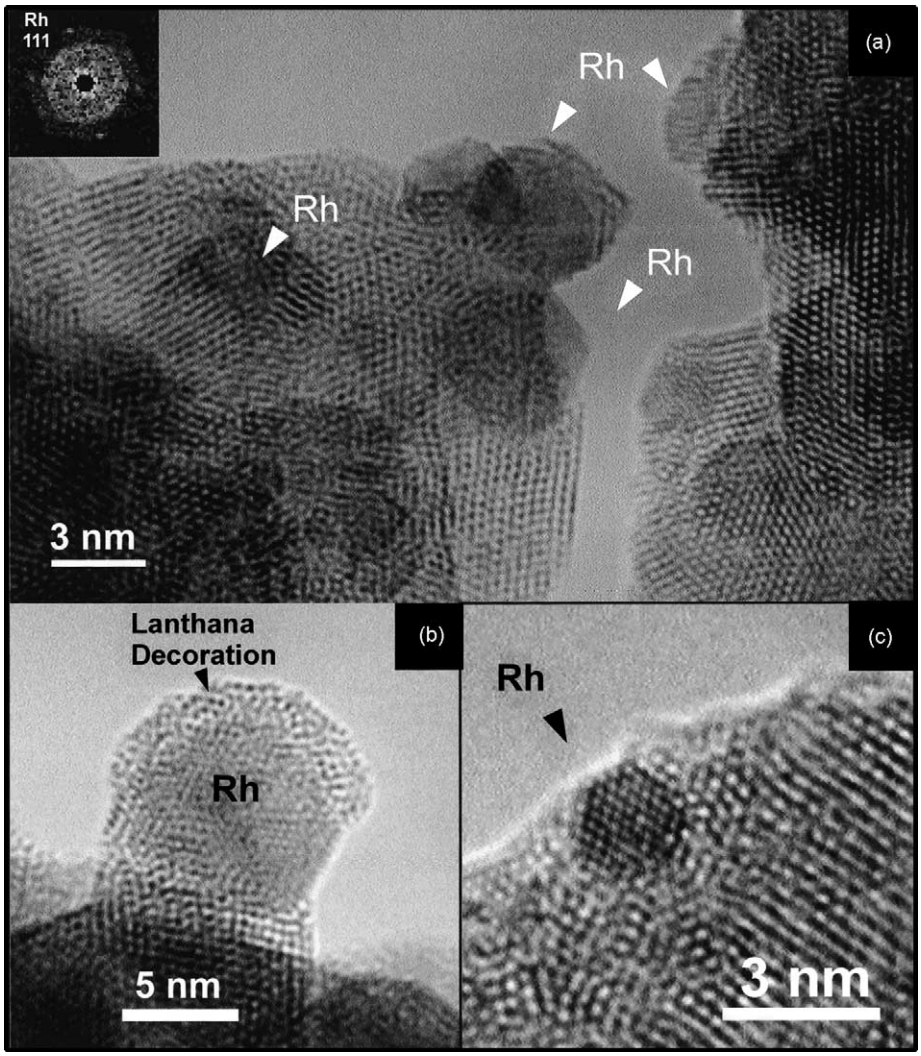

Fig. 8. (a) HREM image showing a general view of a 10% Rh/La_2O_3 catalyst reduced at 773 K; (b) the DDP inset in the figure has been obtained from a small particle. HREM detail showing a rhodium particle decorated by a support overlayer; (c) HREM detail showing a small metal particle on a lanthana background.

non-aqueous solvents to prepare the impregnating solution; (2) depositing the metal phase by direct evaporation under vacuum; (3) using a basic metal precursor. HREM images of catalysts prepared using any of these strategies show, after reduction at low temperature (473 K), the presence of metal particles, Figs. 10–12. Note however that these particles are to some extent decorated because the decomposition of the support during the reduction cannot be avoided.

Summarising the results presented in this section, electron microscopy investigations clearly point out that the chemisorption behaviour of metal catalysts supported on lanthanide sesquioxides is intimately related with the details of the nanostructure of the catalysts, which is tailored during the preparation procedure according to the intrinsic basic character of this family of oxides, but not to their reduction under very mild conditions.

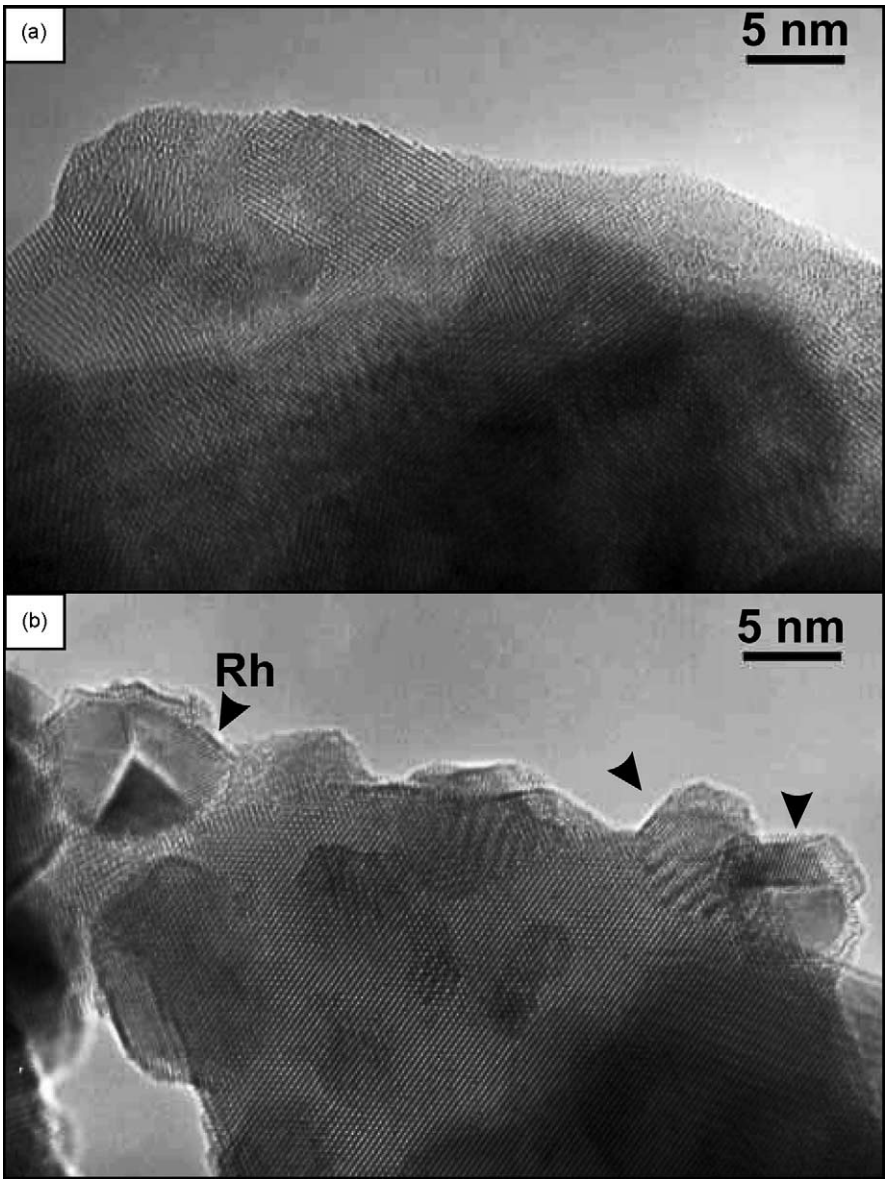

Fig. 9. HREM images corresponding to: (a) a 5.4% Rh/Sm_2O_3 catalyst reduced at 773 K; (b) the same catalyst sample further heated in a flow of He at 1173 K (notice the existence of encapsulated rhodium particles).

4. SMSI-like effect in M/CeO_2 and related catalytic systems

Consequently to the generalised application of TWC (three-way catalyst) devices in the control of the exhaust emissions from spark-ignited motor vehicles [17], for the last decade, most of the studies dealing with the SMSI effect have been focused on NM/CeO_2 (NM: noble metal) and related catalytic systems ($NM/CeMO_{2-x}$). In accordance with recent review works [18,19], these studies have considered three major problems: (1) The experimental difficulties to

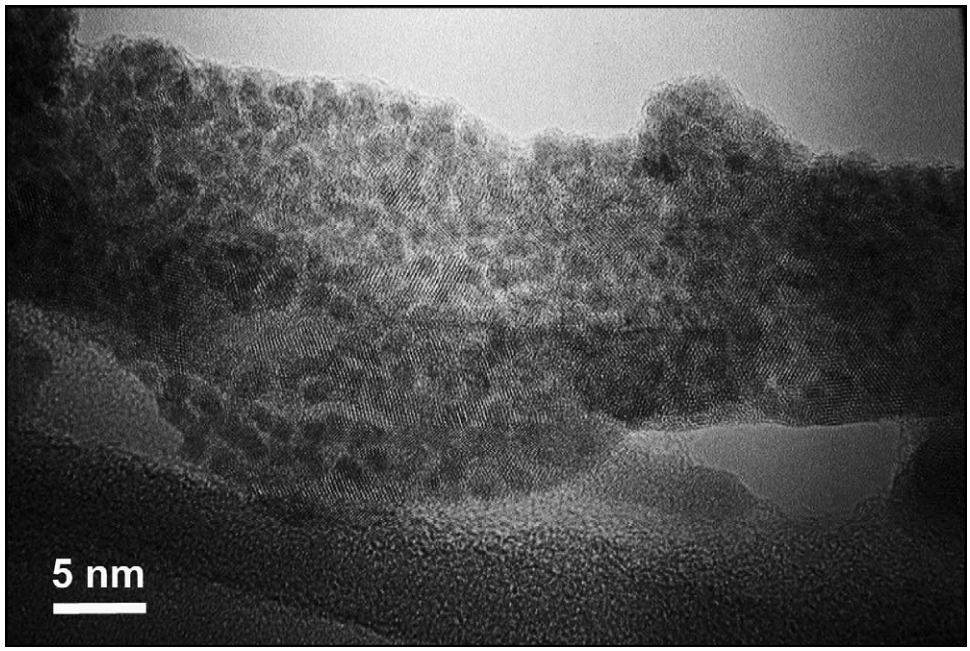

Fig. 10. HREM image showing a general view of a Rh/La_2O_3 catalyst prepared by vacuum deposition after reduction at 473 K.

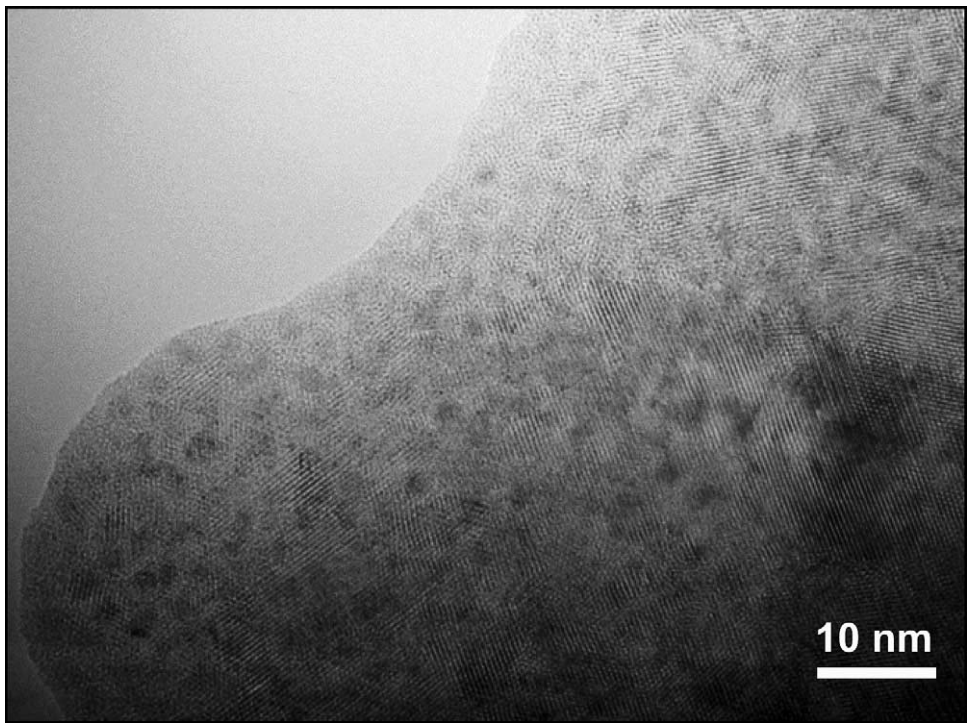

Fig. 11. General view of an 8% Rh/La_2O_3 catalyst prepared by impregnation with an acetone solution of $Rh(NO_3)_3$, and further reduced at 473 K.

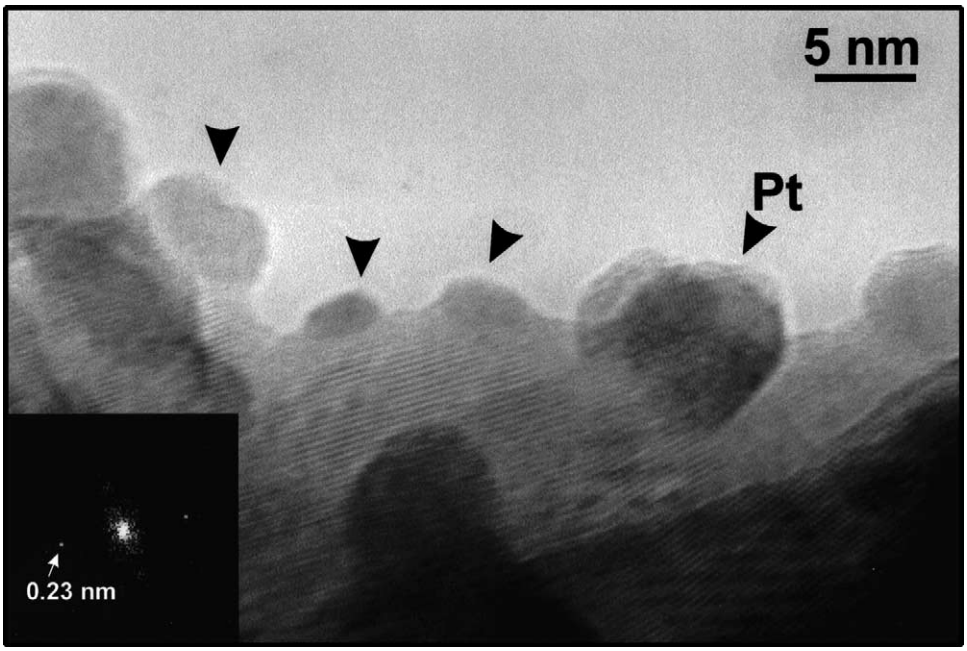

Fig. 12. HREM image of a 3% Pt/La_2O_3 catalyst prepared by impregnation with an aqueous solution of $[Pt(NH_3)_4](OH)_2$, and further reduced at 423 K.

be overcome in order to establish the occurrence of a true SMSI effect. (2) The nano-structural aspects. (3) The chemical aspects. We shall briefly overview these three major questions. Finally, in the light of the experimental information presently available, the most characteristic features of the metal/support interaction phenomena occurring in this family of catalysts will be summarised in the form of a few concluding remarks.

4.1. Experimental problems for establishing the existence of SMSI-like effects in M/CeO_2 and related systems

Establishing the occurrence of a true SMSI effect, as defined by Tauster et al. [1] requires to unequivocally show that metal deactivation is specifically due to its interaction with the support, i.e. several other causes like metal sintering or encapsulation, typically associated with the increase of T_{redn} must be excluded. In the latter respect, it is worth recalling that ceria is known to exhibit a poor textural stability, particularly in the case of high surface area samples ($>50\,m^2\,g^{-1}$), under reducing conditions [20,21]. Accordingly, reduction treatments at 773 K, typically applied in studies on the SMSI effect, may diminish very significantly the BET surface area of ceria, thus inducing metal encapsulation effects. To exclude the occurrence of such a side effect is important, because the inherent metal loss cannot be quantified easily.

Regarding the metal sintering effects, it would be noted that the experimental studies of the metal dispersion are mainly based on volumetric chemisorption measurements, in most of cases of H_2 [6,22,23–29], and occasionally of CO [30–36]. The interpretation of these volumetric data, however, may be greatly disturbed by the simultaneous occurrence of significant, sometimes very important, H_2 [22,28,29,37,38] and CO [39–43] chemisorption on the ceria-based supports. Moreover, this parallel adsorption, which would certainly mask the metal contribution, is sensitive to a number of variables like: the redox state of the support [38,44], or the incorporation to ceria of chlorine coming from the metal precursor [24,44]. To summarise, the support contribution to the total amount of the probe molecules chemisorbed by the ceria-based catalysts may vary as a function of the reduction treatment or the nature of the metal precursor.

Likewise, the estimate of the metal dispersion in M/CeO_2 and related systems by using chemical techniques may be complicated by the occurrence of SMSI phenomena. In effect, in the case of catalysts whose behaviour against the reduction temperature is not well-established, the upper T_{redn} limit allowing the catalyst to be reduced without disturbing its chemisorptive properties is not known. This introduces further doubts about the experimental protocol to be followed for determining metal dispersions. We may conclude accordingly, that to have available metal dispersion data other than those obtained from chemical techniques should be a major relevant objective of the studies on the strong metal/support interaction effects. For this purpose, HREM has proved to be a very powerful alternative tool [18,19].

4.2. Nano-structural aspects of the strong metal/support interaction effects in M/CeO_2 and related systems

To have available detailed information about the nano-structural evolution undergone by these catalysts when submitted to both reduction treatments at increasing temperatures, and different re-oxidation/re-reduction treatments aimed at regenerating the deactivated samples, is critically important to establish the occurrence and specific characteristics of the metal/support interaction phenomena they may exhibit. As stated above, HREM has played a major role in this kind of studies. Firstly, it has been used to determine the metal particle size distribution, i.e. the metal dispersion, associated with each of the treatments above [18,45]. HREM images provide a direct visualisation of the metal particles and allow an estimation of their diameters. From these measurements particle size distributions can be established. As an example, Fig. 13 summarises the evolution with T_{redn} of the metal particle size in a series of ceria-based catalysts. Data obtained for Rh and Pt catalysts supported on both pure CeO_2 and two mixed oxides have been included. As deduced from data plotted in this figure, there are significant differences between the Rh and Pt catalysts, the former showing a better resistance against sintering. Likewise, the nature of the support, CeO_2, $Ce_{0.80}Tb_{0.20}O_{2-x}$ or $Ce_{0.68}Zr_{0.32}O_{2-x}$ does not seem to play a major role in the stabilisation of the dispersed metal phase.

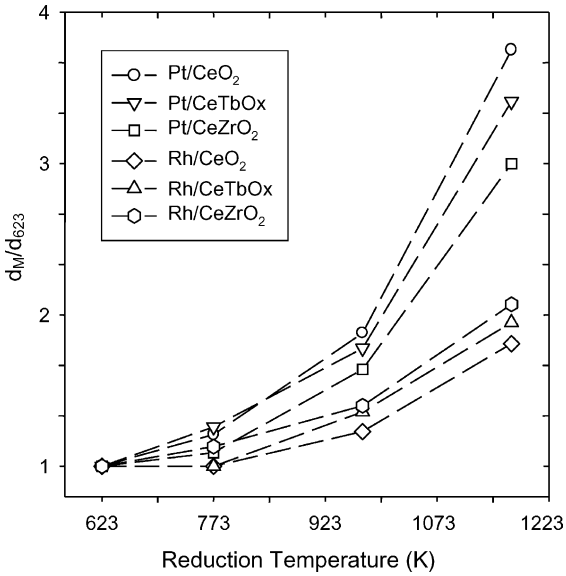

Fig. 13. Evolution with reduction temperature of the particle average diameter for different rhodium and platinum supported catalysts.

HREM has allowed us to obtain some other very fine details of the nano-structural constitution of these catalysts. An important one refers to the chemical state of the small particles. Thus, HREM indicate that for low temperature reduction treatments, Rh and Pt are present in these catalysts as a metallic phase and in the form of nanosized particles, with morphologies close to more or less stepped or rounded cubeoctahedrons. An interesting feature of these small metal particles which have been evidenced from HREM recordings is that they grow on the surface of the support under preferential orientation relationships. Fig. 14 illustrates an example of so-called parallel-orientation relationship [19]. Note in the HREM image, Fig. 14(a), and DDP's in Fig. 14(b) and (c), how the lattice planes in the support run parallel to those of the metal with the same ($h\,k\,l$) indices. This particular orientation relationship is characterised by a parallel alignment of the zone axis with the same indices of the two components of the catalyst.

By using nanodiffraction [46,47], digital processing of the experimental HREM images [4,25], and computer simulation techniques [16], the structural relationships existing in ceria-based and a number of ceria-based mixed oxide supported Rh, Pt and Pd

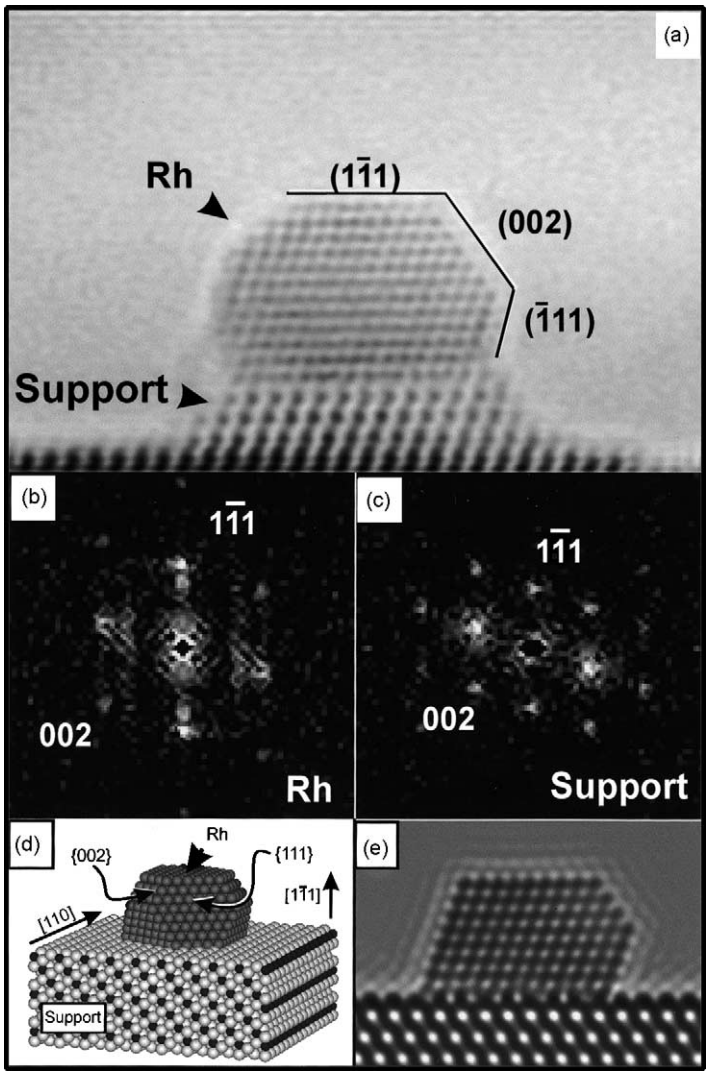

Fig. 14. (a) Experimental image corresponding to a 0.5% Rh/$Ce_{0.8}Tb_{0.2}O_{2-x}$ catalyst reduced at 773 K; (b) DDPs obtained from the contrasts of the metal particle and (c) the support; (d) model showing a rhodium particle grown on the mixed oxide crystal with a parallel orientation relationship; (e) simulated image obtained from the model.

catalysts have been characterised. Profile and plan view HREM images have provided the crystallographic details of these orientation relationships for a variety of contacts between the metal and the support at the interface [19].

HREM has also unequivocally proved the occurrence of metal decoration effects in CeO_2- [18,48,51], $Ce_{0.80}Tb_{0.2}O_{2-x}$- [52], and $Ce_{0.68}Zr_{0.32}O_2$-supported [28,29] Rh, Pt, and/or Pd catalysts. Fig. 15 shows representative examples of decorated rhodium particles as revealed by HREM in a Rh/CeO_2 catalyst, Fig. 15(a) and in a Rh/$Ce_{0.80}Tb_{0.2}O_{2-x}$ sample, Fig. 15(b). These studies have also shown that the reduction temperatures required to induce the partial coverage of the metal crystallites are well above 773 K, typically $T_{redn} \geq 973$ K are necessary to induce this effect. This is a relevant difference between M/CeO_2 and M/TiO_2 systems.

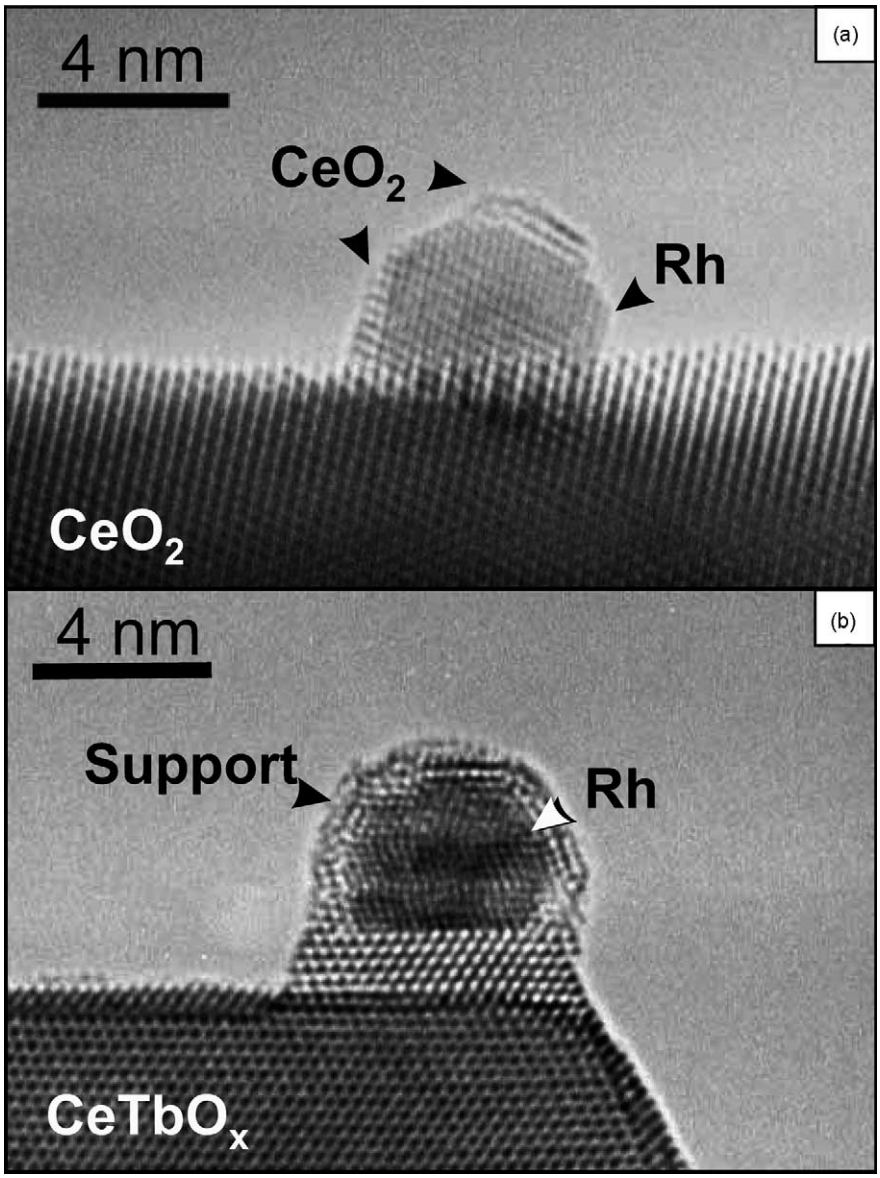

Fig. 15. HREM images corresponding to: (a) a 2.5% Rh/CeO_2 catalyst reduced at 1173 K; (b) a 0.5% $Rh/Ce_{0.8}Tb_{0.2}O_{2-x}$ catalyst reduced at 1173 K.

Regarding once more the chemical nature of the supported particles, though the formation of a Pt–Ce alloy had already been proposed in the pioneering studies on the metal deactivation occurring in a Pt/CeO_2 catalyst reduced at 773 K [31], it was much later when this proposal has been experimentally confirmed. In effect, by analysing the HREM images recorded for a Pt/CeO_2 reduced at very high temperature, 1173 K, contrasts other than those characteristic of ceria and Pt could be observed. They were interpreted as due to a $CePt_5$ intermetallic compound [49]. This inter-metallic phase has also been observed in a $Pt/Ce_{0.80}Tb_{0.20}O_{2-x}$ catalyst reduced at fairly the same temperature [52], i.e. well above

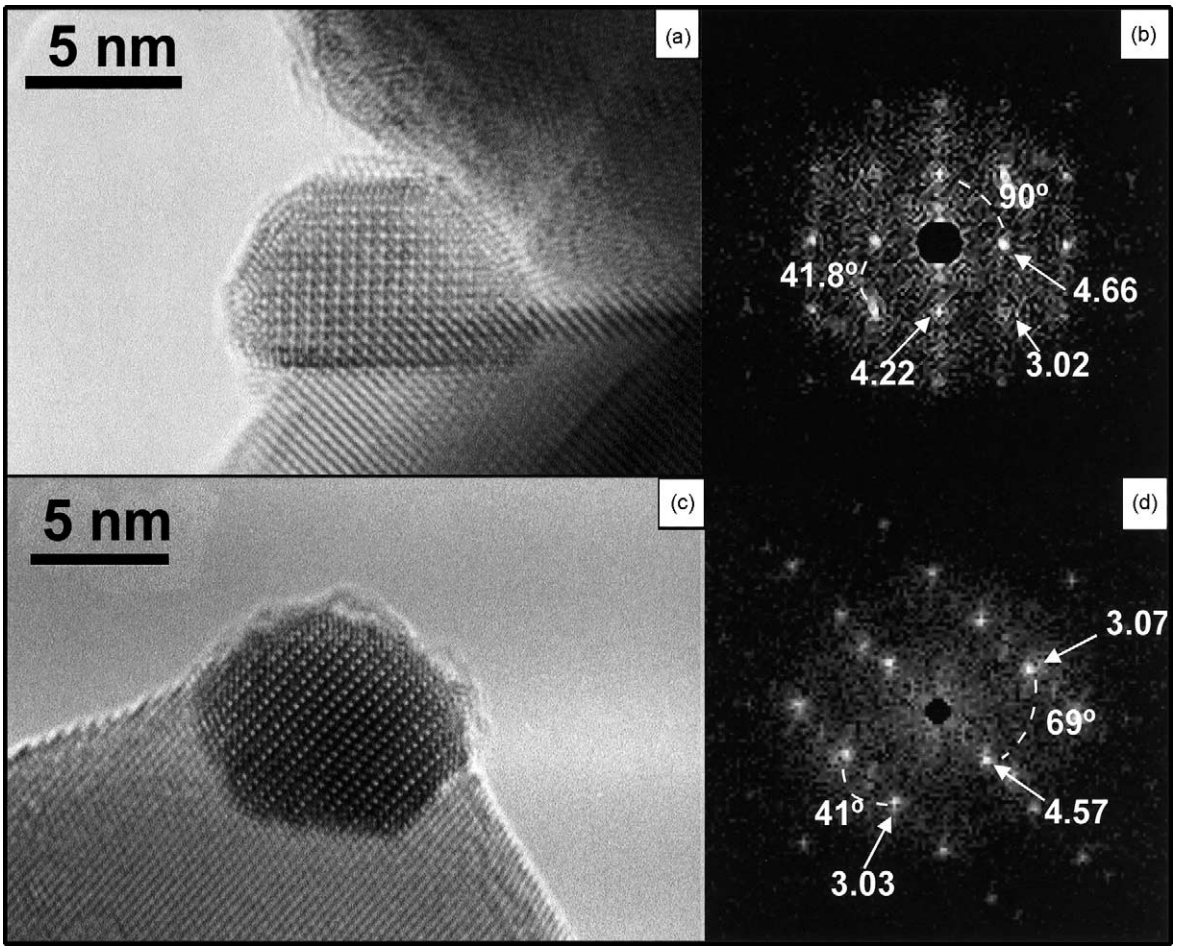

Fig. 16. Experimental HREM images (a and c) and DDPs (b and d) corresponding to a 4% Pt/CeO_2 catalyst (a and b); and to a 5% $Pt/Ce_{0.8}Tb_{0.2}O_{2-x}$ catalyst (c and d). Both catalysts were reduced at 1173 K. *d*-Spacing values of 4.6, 4.2 and 3.0 Å correspond to (0 0 1), (1 0 0) and (1 0 1) planes of $LnPt_5$ phase. DDPs (b) and (d) can be indexed as [0 1 0] and [0 1 1] zone axis for $LnPt_5$ phase.

those proposed in [31]. Fig. 16 shows two HREM images corresponding to these catalysts. Note in this case the dramatic changes in the contrasts of the supported particles with respect to those characteristic of metallic f.c.c. particles observed after reduction at low temperatures, as it is the case of the particle shown in Fig. 14. Substantial changes in the fringe spacings and geometry are observed.

The formation of this intermetallic phase has also been confirmed by direct chemical analysis of the supported particles present in Pt catalyst reduced at temperatures above 1173 K. In [52], by using a nanoprobe and electron energy loss spectroscopy (EELS), the incorporation of the lanthanide elements into the supported particles has been confirmed. Figs. 17 and 18 illustrate this conclusion. Note at this respect how the EELS spectrum obtained from a location inside the supported particle far from the interface contains the M4, M5 peaks of the lanthanides, as in the support. Moreover, the comparative analysis of the Ce–M4, M5 peaks in the support and the particle indicate, Fig. 18, a 1.8 eV shift of these peaks towards lower energies in the particle as well as a substantial change in the relative intensities of these two peaks. These modifications in the fine structure evidence a change in the oxidation state of cerium from that characteristic of

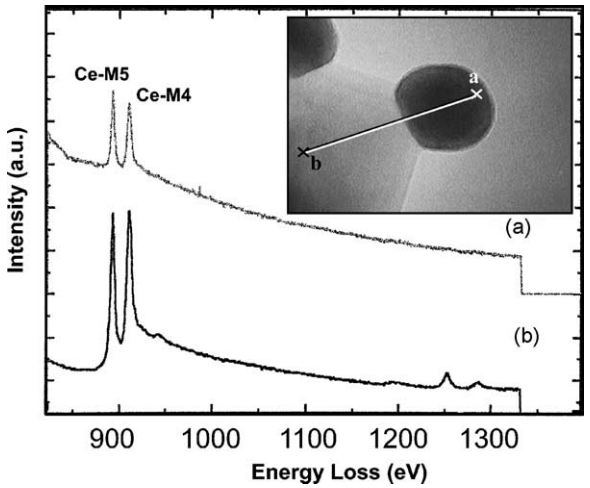

Fig. 17. Electron energy loss spectra recorded on a 5% $Pt/Ce_{0.8}Tb_{0.2}O_{2-x}$ catalyst reduced at 1173 K. Signals corresponding, respectively, to the analysis of a supported particle (a) and the support (b).

CeO_2 (formally +4) to that observed in compounds like γ-Ce or CePd (formally 0). All these changes are in fact those expected for the formation of an intermetallic.

A final feature regarding the formation of this intermetallic compounds worth being highlighted is the behaviour of a $Pt/Ce_{0.68}\ Zr_{0.32}O_2$ catalyst [19].

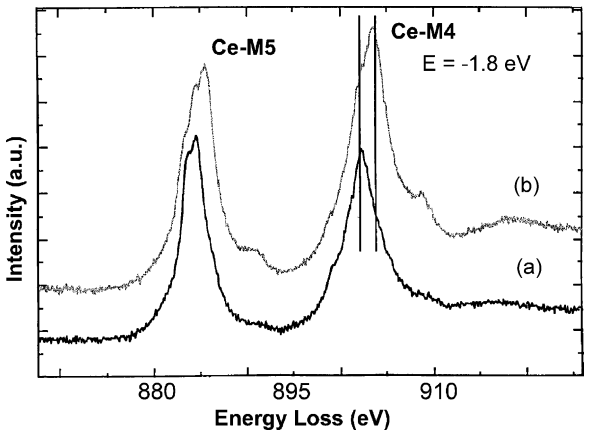

Fig. 18. Electron energy loss spectra recorded on a 5% $Pt/Ce_{0.8}Tb_{0.2}O_{2-x}$ catalyst reduced at 1173 K in the energy range corresponding to Ce–$M_{4,5}$ lines for a supported particle (a) and the support (b).

In contrast to that observed on pure ceria or on a $Ce_{0.8}Tb_{0.2}O_{2-x}$ mixed oxide, the formation of the intermetallic phase does not take place, even after prolonged reduction at 1223 K. This result suggests that zirconium stabilises reduced cerium species within the fluorite structure and precludes its incorporation into the metal f.c.c. lattice to form the intermetallic phase.

On Pd/CeO_2, the occurrence of an alloy phase has also been suggested [50,51]. However, no intermetallic compounds with well-defined stoichiometry and crystallography could be identified, the proposal being mainly supported by the distortions observed in the parameters characterising the Pd unit cell. Regarding the ceria-supported Rh catalysts, alloying effects have never been reported to occur.

A very important aspect of the nano-structural characterisation of M/CeO_2 catalysts is the investigation of the evolution undergone by decorated and alloyed samples when submitted to different re-oxidation treatments followed by re-reduction at a mild temperature. These HREM studies, which were aimed at gaining information about the regeneration behaviour of the catalysts, have provided very interesting data [18,19,45,48,53]. Figs. 19 and 20 summarise the major findings about this particular topic.

In the case of rhodium, re-oxidation at 773 K of the catalyst previously reduced at high temperature results in the formation of large and rounded polycrystalline particles which present lattice spacings in the range 0.24–0.29 nm, characteristic of the oxidised forms of rhodium, Fig. 19(a). Detailed EELS analysis at atomic scale have proved the presence of cerium within these particles [53]. Re-reduction at 473 K of the oxidised sample produces a catalyst in which metallic rhodium particles appear decorated by ceria layers, Fig. 19(b).

Regarding Pt catalysts, re-oxidation at 673 K of the intermetallic phase detected after high temperature reduction results also in large, polycrystalline particles which, according to lattice fringe analysis, consist of a core made of a few metallic platinum units surrounded by an outer shell constituted by an ensemble of randomly oriented, plate-like, CeO_2 nanocrystallites. Most of the surface of the metallic core seems to be covered, Fig. 20(a). Re-reduction at low temperature does not modify significantly the structure of the catalyst. Only a subtle improvement in the faceting of the metallic cores is appreciated, which results in less rounded supported particles, Fig. 20(b). This suggests

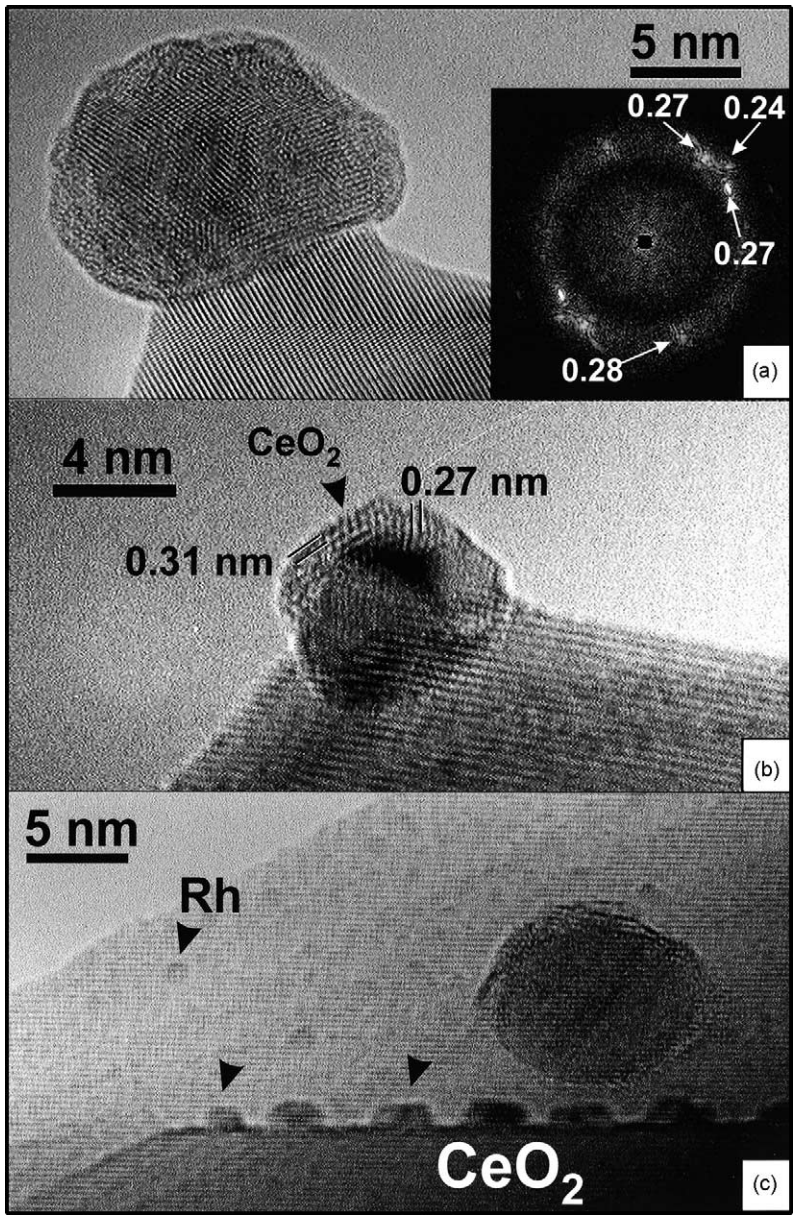

Fig. 19. Experimental HREM images corresponding to: (a) a 2.5% Rh/CeO_2 catalyst reduced at 1173 K and further oxidised at 773 K. (b) Sample (a) further re-reduction at 623 K. (c) The same 2.5% Rh/CeO_2 catalyst reduced at 1173 K, and further re-oxidised at 1173 K. *d*-Spacing values of 0.31 and 0.27 nm in (b) are associated to (1 1 1) and (2 0 0) planes of CeO_2 structure.

that prior to re-reduction the surface of the Pt core could be partially oxidised.

Thus, the research program developed on Rh/CeO_2 and Pt/CeO_2 catalysts reduced at 1173 K has shown that the classic re-oxidation treatment at 773 K, which is well known to recover the M/TiO_2 catalysts from the SMSI state, does not allow the ceria-supported catalysts to be regenerated. By contrast, the above-mentioned treatment leads to the formation of large polycrystalline aggregates consisting of ceria

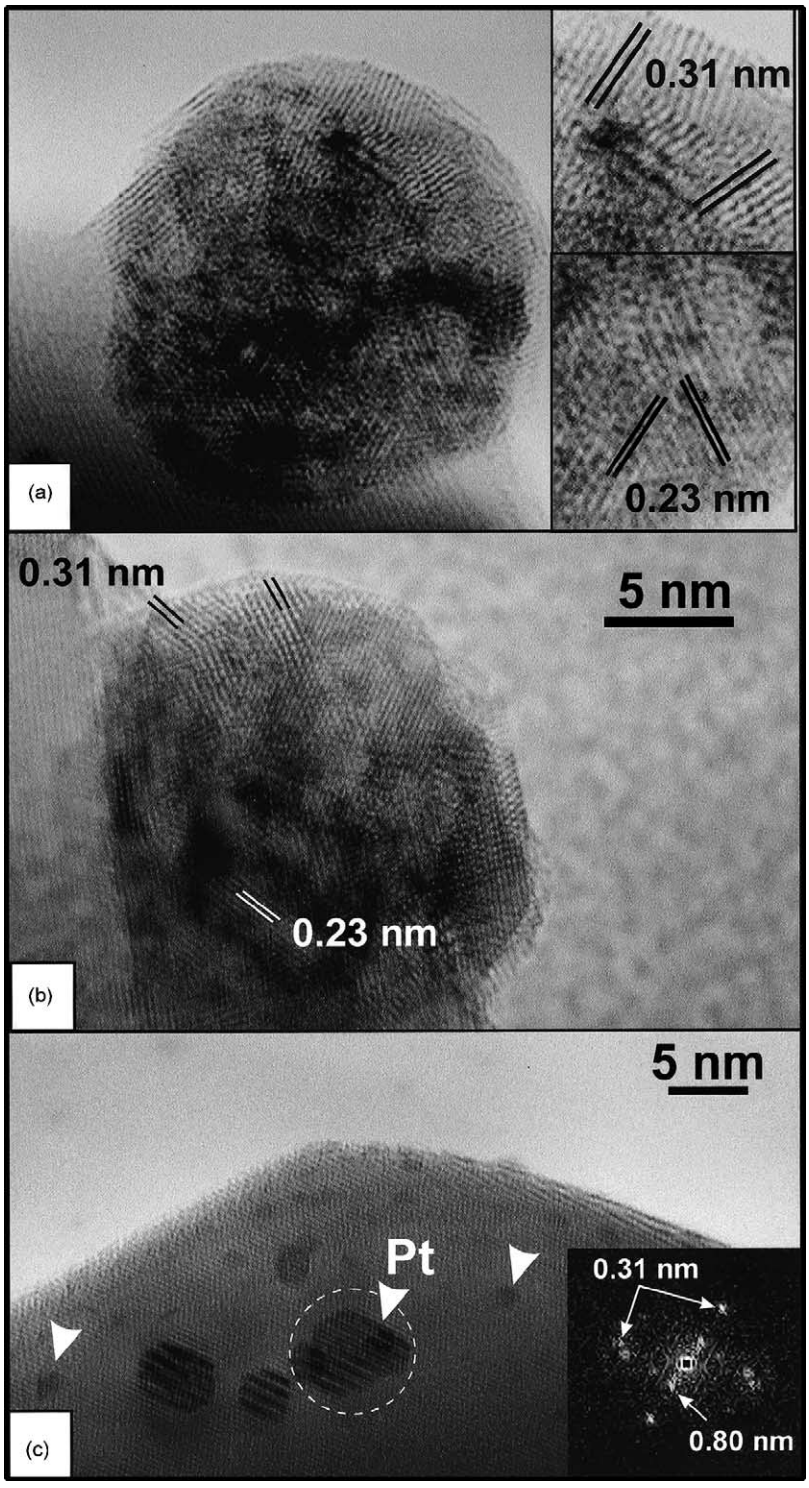

Fig. 20. Experimental HREM images corresponding to: (a) a 4% Pt/CeO_2 catalyst reduced at 1173 K and further oxidised at 773 K. (b) Sample (a) further reduced at 623 K. (c) The same 4% Pt/CeO_2 catalyst reduced at 1173 K and further re-oxidised at 1173 K. *d*-Spacing values of 0.31 and 0.23 nm correspond to (1 1 1) planes for CeO_2 and Pt structures, respectively.

and oxidised forms of the metal. If these re-oxidised samples are further reduced at $T_{redn} \leq 623$ K, no segregation of metal and support occurs, thus resulting aggregates in which CeO_2 and the reduced noble metal coexist. As shown in [53], to fully revert the decorated/alloyed state, much higher re-oxidation temperatures have to be applied, Figs. 19(c) and 20(c). These drastic treatments, however, strongly modify the metal size distribution. Currently available size distribution studies using HREM and SEM/EDS, indicate a redispersion effect in the case of supported Rh, whereas in the case of the Pt catalysts a strong sintering effect takes place in parallel to the recovery from the alloyed state.

4.3. Chemical aspects of the SMSI-like effects in M/CeO$_2$ and related systems

The occurrence of significant chemical perturbations in M/CeO_2 and related systems when reduced at increasing temperatures is presently well-documented. Also worth of outlining is that partial deactivation effects are generally observed, complete inhibition of the metal chemisorptive properties being very seldom reported. The experimental evidence for these chemical perturbations comes from H_2 [6,17,18,23,25,26,28,29] and CO [17,30–36,54] chemisorption studies, but also from catalytic activity measurements [6,23,31,51,55–58]. In the latter case, a number of reactions including hydrocarbon hydrogenolysis [6,31,51,55], and benzene [51], acetone [6,56], crotonaldehyde [56], and CO and CO_2 [6,23,55,58] hydrogenations have been investigated. In most of these studies $T_{redn} \leq 773$ K. If the nano-structural information reported above is recalled, this is a remarkable observation. In effect, within this range of reduction temperatures, neither decoration nor alloying phenomena should be expected to occur. Moreover, data in Fig. 13 suggest that, if textural properties of the support are not significantly modified by the reduction treatments, changes in the metal dispersion should also be very moderate.

Drawing meaningful conclusions about the influence of T_{redn} on the chemisorptive behaviour of M/CeO_2 and related systems requires a very careful analysis of the experimental data. Thus, when using H_2 to probe the chemical behaviour of the supported metal, the likely occurrence of spillover phenomena

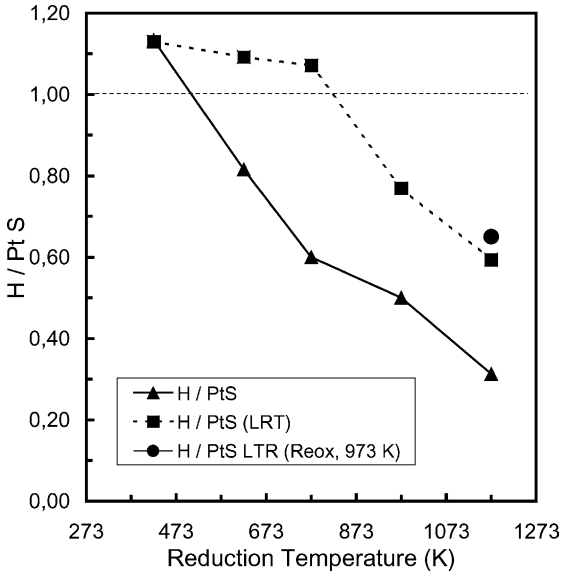

Fig. 21. Ratio between metal dispersion data as determined from H_2 chemisorption (H/Pt$_t$) and as determined by HREM (Pt$_s$/Pt$_t$): (H/Pt$_t$)(Pt$_s$/Pt$_t$) = H/Pt$_s$, for Pt/$Ce_{0.68}Zr_{0.32}O_2$. (▲) Samples reduced at the indicated temperatures, (■) samples reduced at the indicated temperatures, then re-oxidised at 700 K and further re-reduced at 423 K (LTR), (●) sample reduced at 1173 K, then re-oxidised at 973 K and further re-reduced at 423 K (LTR).

should always be considered. It is also worth recalling that these phenomena are very sensitive to the reduction/evacuation conditions, as well as to the nature of the metal precursor [18,59]. Several experimental alternatives have been used to minimise spillover contribution. Among them, hydrogen chemisorption at 191 K [22,28,29], and isotopic transient kinetic (ITK) studies, at 298 K. of the H_2/D_2 exchange [18], have shown to be useful approaches. As an example, Fig. 21 summarises the results recently published about the evolution with T_{redn} of the metal chemisorption capability of a Pt/$Ce_{0.68}Zr_{0.32}O_2$ catalyst, as determined by volumetric studies at 191 K [29]. This catalyst, which was prepared from a chlorine free metal precursor, has a low surface area (20 $m^2\,g^{-1}$) and a high textural stability.

To detect the likely occurrence of Pt deactivation effects, in [29] H/Pt$_s$ data are plotted against T_{redn}. H/Pt$_s$ parameter accounts for the number of H atoms chemisorbed, at 191 K, per surface Pt atom (Pt$_s$). This parameter may be estimated as the ratio D_H/D_{HREM}, where D_H (H/Pt$_t$; Pt$_t$: total number of Pt atoms in the

catalyst sample) would measure the metal dispersion as determined by hydrogen chemisorption at 191 K; D_{HREM} (Pt_s/Pt_t) accounting for the metal dispersion as deduced from HREM [45]. In accordance with the meaning of the $D_H/D_{HREM} = H/Pt_s$ parameter, and assuming a 1:1 adsorption stoichiometry ratio within the whole range of particle size of interest, its value should be constant and equal to 1 with independence of the actual metal dispersion. In other words, the H/Pt_s ratio takes into account the likely occurrence of some metal sintering upon increasing T_{redn}. By contrast, $H/Pt_t < 1$ would indicate the occurrence of deactivation effects other than the metal sintering. Metal encapsulation may be disregarded because of the high textural stability of the investigated catalyst. In fact, its BET surface area does not change significantly within the whole range of reduction temperatures. Accordingly, the progressive decrease of H/Pt_s values, which is noticeable at $T_{redn} = 623$ K, and very significant at 773 K, may be interpreted as due to the occurrence of a metal/support interaction effect. Taking into account that no significant nano-structural changes are observed on the catalyst reduced at or below $T_{redn} = 773$ K, we should conclude that electronic perturbations play a major role in the deactivation of the Pt crystallites. This conclusion is in agreement with that obtained from some recent studies on Pt/CeO_2 [18,54]. It is also supported by the results shown in Fig. 21 (points linked by the dotted line) about the effect of the re-oxidation treatment at 673 K (400 °C) followed by reduction at room temperature, which was applied to the catalysts initially reduced at each of the investigated temperatures.

In [28] a study, parallel to the one reported above, has been carried out on a $Rh/Ce_{0.68}Zr_{0.32}O_2$ catalyst. The mixed oxide support was the same as the one used in [29]. Likewise, a free from chlorine Rh precursor was used. Metal dispersions of Pt and Rh catalysts reduced at 473 K were also close to each other. In contrast to that reported for the Pt catalyst, no significant Rh deactivation could be detected for $T_{redn} \leq 773$ K, the effect being moderate even for $T_{redn} > 773$ K. We may conclude accordingly, that metal/support interaction effects in $NM/Ce_{0.68}Zr_{0.32}O_2$ catalysts are sensitive to the nature of noble metal, being stronger in the case of the Pt samples. This observation is relevant in relation to the choice of the reduction temperature to be applied for obtaining meaningful dispersion data from low-temperature hydrogen chemisorption studies.

4.4. Concluding remarks

The capability of electron probe based analysis to unveil the ultimate details of the nanostructure of catalytic materials has been proved. The combined application of structural and chemical analysis techniques at the nanoscale by using HREM, SEM and EELS spectroscopy appears as a very powerful tool to characterise catalytic materials and to understand their macroscopic behaviour. In relation with the metal–support interaction effects, though there are still many questions on their precise nature to be satisfactorily answered, for the last decade some significant progress has been made in their understanding.

In the particular case of ceria-based catalytic systems, the combination of chemical and nano-structural information presently available has allowed to propose a model to understand the observed effects. According to this model, the chemical and nano-structural evolution undergone by M/CeO_2 and related systems when applying increasing reduction temperatures qualitatively resembles the one previously reported for M/TiO_2 catalysts. There are, however, some significant differences. Firstly, all the HREM studies have agreed on the absence of metal decoration for $T_{redn} \leq 773$ K. For M/CeO_2 catalysts, reduction temperatures well above those required in the case of M/TiO_2, typically 973 K, have to be applied to induce such a characteristic nano-structural feature of the SMSI effect. Secondly, M–Ce alloying could only be unequivocally established at very high reduction temperatures. Therefore, its contribution to the metal deactivation effects observed on catalysts reduced at $T_{redn} \leq 773$ K seems to be very unlikely. To summarise, if some other contributions, like those related to the metal sintering or encapsulation, may be excluded, metal deactivation occurring at moderate reduction temperatures ($T_{redn} \leq 773$ K) should reasonably be interpreted as due to electronic perturbations associated with the interaction between the metal micro-crystals and the reduced ceria support.

Also worth of outlining are the differences observed between M/TiO_2 and M/CeO_2 catalysts in relation to the treatments allowing recovering them from the deactivated state. For the titania-supported

catalysts, as already noted, re-oxidation at 773 K followed by a mild reduction are typical regeneration conditions. By contrast, the recovery of the M/CeO_2 catalysts from a decorated or alloyed state requires far higher re-oxidation temperatures. Consequently, if re-oxidation treatments at $T_{redn} \leq 773$ K induce the regeneration of a deactivated M/CeO_2 catalysts, the most likely interpretation is that neither decoration nor alloying are playing a relevant role, the observed chemical perturbations being mainly due to electronic effects.

Finally, the peculiar behaviour of the metal-supported on lanthanide sesquioxide, has a neatly different origin. Rather than the reducibility, the basic character of these oxides is the key property which influences the nanostructure of these catalysts. The details of the procedure employed to deposit the metal phase onto these support determine the final state of the metal and its relationship with the support. A model has been proposed, based on the well-established chemical properties of 4f-sesquioxides, which allows understanding their peculiar chemisorption behaviour. In this model, the formation of a highly dispersed metal phase after the first steps of the preparation procedure, mixed at atomic level with the support oxide, is the main feature.

Acknowledgements

This contribution has been supported by the CICYT (projects MAT-99-0570 and MAT-2002-02782), and the Junta de Andalucía. The HREM images presented in this work were obtained at the Electron Microscopy Facilities of UCA.

References

[1] S.J. Tauster, S.C. Fung, R.L. Garten, J. Am. Chem. Soc. 100 (1978) 170.
[2] S.J. Tauster, Acc. Chem. Res. 20 (1987) 389.
[3] G.L. Haller, D.E. Resasco, Adv. Catal. 36 (1989) 173.
[4] A.K. Datye, D. Kalakkad, M.H. Yao, D.J. Smith, J. Catal. 155 (1995) 149.
[5] C. Binet, A. Jadi, J.C. Lavalley, M. Boutonet-Kizling, J. Chem. Soc., Faraday Trans. 88 (1992) 2079.
[6] A. Trovarelli, G. Dolcetti, C. Leitenburg, J. Kaspar, P. Finetti, A. Santoni, J. Chem. Soc., Faraday Trans. 88 (1992) 1311.
[7] A.D. Logan, E.J. Braunschweig, A.K. Datye, D.J. Smith, Langmuir 4 (1988) 827.
[8] E.J. Braunschweig, A.D. Logan, A.K. Datye, D.J. Smith, J. Catal. 118 (1989) 227.
[9] S. Bernal, F.J. Botana, J.J. Calvino, C. López, J.A. Pérez Omil, J.M. Rodríguez-Izquierdo, J. Chem. Soc., Faraday Trans. 92 (1996) 2799.
[10] J. Sanz, J.P. Belzunegui, J.M. Rojo, J. Am. Chem. Soc. 114 (1992) 6749.
[11] C. Hippe, R. Lamber, G. Schulz-Ekloff, U. Schubert, Catal. Lett. 43 (1997) 195.
[12] R.F. Hicks, Q.-J. Yen, A.T. Bell, J. Catal. 89 (1984) 498.
[13] J. Zhu, G.A. Somorjai, Nano Lett. 1 (2001) 8.
[14] S. Bernal, M. Cauqui, J.M. Gatica, C. Larese, C. López Cartes, unpublished results.
[15] S. Bernal, J.J. Calvino, C. López-Cartes, J.A. Pérez Omil, J.M. Pintado, J.M. Rodríguez-Izquierdo, K. Hayek, G. Rupprechter, Catal. Today 52 (1999) 29.
[16] S. Bernal, F.J. Botana, J.J. Calvino, G.A. Cifredo, R. García, J.M. Rodríguez-Izquierdo, Ultramicroscopy 34 (1990) 60.
[17] A. Trovarelli, Catal. Rev. Sci. Eng. 38 (1996) 439.
[18] S. Bernal, J.J. Calvino, M.A. Cauqui, J.M. Gatica, C. Larese, J.A. Pérez-Omil, J.M. Pintado, Catal. Today 50 (1999) 175.
[19] S. Bernal, J.J. Calvino, J.M. Gatica, C. Lopez-Cartes, J.M. Pintado, in: A. Trovarelli (Ed.), Catalysis by Ceria and Related Materials, Catalytic Science Series, vol. 2, Imperial College Press, Chapter 4, 2002, pp. 85–168.
[20] V. Perrichon, A. Laachir, G. Bergeret, R. Frety, L. Tournayan, O. Touret, J. Chem. Soc., Faraday Trans. 90 (1994) 773.
[21] M. Pijolat, M. Prin, M. Soustelle, O. Touret, P. Nortier, J. Chem. Soc., Faraday Trans. 91 (1995) 3941.
[22] S. Bernal, F.J. Botana, J.J. Calvino, M.A. Cauqui, G.A. Cifredo, A. Jobacho, J.M. Pintado, J.M. Rodríguez-Izquierdo, J. Phys. Chem. 97 (1993) 4118.
[23] C. de Leitenburg, A. Trovarelli, J. Kaspar, J. Catal. 166 (1997) 98.
[24] D.I. Kondarides, X.E. Verykios, J. Catal. 174 (1998) 52.
[25] P. Fornasiero, J. Kaspar, M. Graziani, J. Catal. 167 (1997) 576.
[26] A. Pfau, J. Sanz, K.D. Schiervaum, W. Göpel, J.P. Belzunegui, J.M. Rojo, Stud. Surf. Sci. Catal. 101 (1996) 931.
[27] P.J. Levy, M. Primet, Appl. Catal. 70 (1991) 263.
[28] J.M. Gatica, R.T. Baker, P. Fornasiero, S. Bernal, G. Blanco, J. Kaspar, J. Phys. Chem. B 104 (2000) 4667.
[29] J.M. Gatica, R.T. Baker, P. Fornasiero, S. Bernal, J. Kaspar, J. Phys. Chem. B 105 (2001) 1191.
[30] S.E. Golunski, H.A. Hatcher, R.R. Rajaram, T.J. Truex, Appl. Catal. B 5 (1995) 367.
[31] P. Meriaudeau, J.F. Dutel, M. Dufaux, C. Naccache, Stud. Surf. Sci. Catal. 11 (1982) 95.
[32] D.W. Daniel, J. Phys. Chem. 92 (1988) 3891.
[33] M. Primet, M. El Azhar, R. Frety, M. Guenin, Appl. Catal. 59 (1990) 153.
[34] A. Bensalem, J.C. Muller, D. Tessier, F. Bozon-Verduraz, J. Chem. Soc., Faraday Trans. 92 (1996) 3233.
[35] C. Binet, A. Jadi, J.C. Lavalley, M. Boutonet-Kizling, J. Chem. Soc., Faraday Trans. 88 (1992) 2079.

[36] J. Cunningham, D.S. Cullinane, J. Sanz, J.M. Rojo, J. Soria, J.L.G. Fierro, J. Chem. Soc., Faraday Trans. 88 (1992) 3233.
[37] J.L.G. Fierro, J. Soria, J. Sanz, J.M. Rojo, J. Solid State Chem. 66 (1987) 154.
[38] S. Bernal, J.J. Calvino, G.A. Cifredo, J.M. Gatica, J.A. Pérez Omil, J.M. Pintado, J. Chem. Soc., Faraday Trans. 89 (1993) 3499.
[39] S. Bernal, F.J. Botana, J.J. Calvino, G.A. Cifredo, R. García, J.M. Rodríguez-Izquierdo, Catal. Today 2 (1988) 653.
[40] A. Badri, C. Binet, J.C. Lavalley, J. Phys. Chem. 100 (1996) 8363.
[41] C. Li, Y. Sakata, T. Arai, K. Domen, K. Maruya, T. Onishi, J. Chem. Soc., Faraday Trans. 85 (1989) 929.
[42] C. Li, Y. Sakata, T. Arai, K. Domen, K. Maruya, T. Onishi, J. Chem. Soc., Faraday Trans. 85 (1989) 1451.
[43] F. Bozon-Verduraz, A. Bensalem, J. Chem. Soc., Faraday Trans. 90 (1994) 653.
[44] S. Bernal, J.J. Calvino, G.A. Cifredo, J.M. Rodríguez-Izquierdo, J. Phys. Chem. 99 (1995) 11794.
[45] S. Bernal, J.J. Calvino, M.A. Cauqui, J.A. Pérez-Omil, J.M. Pintado, J.M. Rodríguez-Izquierdo, Appl. Catal. B 16 (1998) 127.
[46] M. Pan, J.M. Cowley, R. García, Micron Microsc. Acta 18 (1987) 165.
[47] L. Kepinski, Catal. Today 50 (1999) 237.
[48] S. Bernal, F.J. Botana, J.J. Calvino, G.A. Cifredo, J.A. Pérez-Omil, J.M. Pintado, Catal. Today 23 (1995) 219.
[49] S. Bernal, J.J. Calvino, J.M. Gatica, C. Larese, C. López-Cartes, J.A. Pérez Omil, J. Catal. 169 (1997) 510.
[50] L. Kepinski, M. Wolcyrz, Appl. Catal. A 150 (1997) 197.
[51] L. Kepinski, M. Wolcyrz, J. Okal, J. Chem. Soc., Faraday Trans. 91 (1995) 507.
[52] G. Blanco, J.J. Calvino, M.A. Cauqui, P. Corchado, C. López-Cartes, J.A. Pérez Omil, Chem. Mater. 11 (1999) 3610.
[53] S. Bernal, G. Blanco, J.J. Calvino, C. López-Cartes, J.A. Pérez-Omil, J.M. Gatica, O. Stephan, C. Colliex, Catal. Lett. 76 (2001) 131.
[54] S. Bernal, G. Blanco, J.M. Gatica, C. Larese, H. Vidal, J. Catal. 200 (2002) 411.
[55] D. Kalakkad, A.K. Datye, H. Robota, Appl. Catal. B 1 (1992) 191.
[56] J. Cunningham, S. O'Brien, J. Sanz, J.M. Rojo, J. Soria, J.L.G. Fierro, J. Mol. Catal. 57 (1990) 379.
[57] A. Sepúlveda, F. Coloma, F. Rodríguez-Reinoso, J. Catal. 178 (1998) 649.
[58] C. de Leitenburg, A. Trovarelli, J. Catal. 156 (1995) 171.
[59] M.G. Basallote, S. Bernal, J.M. Gatica, M. Pozo, Appl. Catal. A 232 (2002) 39.